Some shock tube experiments on the chemical kinetics of air at high temperatures

By SAUL FELDMAN
AVCO Research Laboratory, Everett, Massachusetts

(*Received* 1 *March* 1957 *and in revised form* 15 *August* 1957)

SUMMARY

This paper is concerned with the rates at which atoms and molecules react in the air that flows over a body flying through the atmosphere at hypersonic speeds. Using air as a working fluid, a series of shock tube experiments were carried out to provide information about these rates. Mach angle measurements were made to determine the state of the gas in three situations of interest.

(*a*) Flow over flat plates was used to determine the state of the gas behind the incident normal shock; temperatures in the gas that passed through the shock varied between 2000 and 6000° K and densities between standard and 1/80 of standard density.

(*b*) Flow over wedges was employed to decelerate the flow behind the incident shock to a small supersonic Mach number; here temperatures downstream of the oblique shock increased, at most, 2000° K above the free stream value.

(*c*) A Prandtl–Meyer expansion was used to cool rapidly the dissociated gas, so that the recombination process could be investigated; temperatures dropped at most 2500° K and the densities varied between standard and 1/200 of the standard value. In some cases, the initial degree of dissociation of air was over 45%.

The results (figure 11) indicate that the dissociation and recombination relaxation times of the chemical species found in air are very fast, when compared to the time it takes a particle of gas to flow either around a blunt body in hypersonic flight or past small models in shock tubes. Thus the shock tube is shown to be an instrument capable of supplying air at high temperatures in thermodynamic equilibrium (figure 5).

In the case of a non-melting blunt body of about 1 ft. diameter flying through the atmosphere at hypersonic speeds, the present results imply that, when the gas behind the detached shock is in thermodynamic equilibrium, the flow will also be in equilibrium as it expands around the body, provided its speed is greater than 10 000 ft./sec at altitudes below 180 000 ft. (figure 12).

1. Introduction

The kinetic energy of a blunt object flying through the atmosphere at hypersonic speeds is sufficient to dissociate the oxygen and some of the nitrogen in air. At high enough velocities, some of the molecules will also be ionized. These phenomena occur when the gas particles cross the standing bow shock that moves with the body.

Consider a body entering the atmosphere from space. At the point where the velocity is 25 000 ft./sec and the altitude is 140 000 ft., the stagnation point temperature could be anywhere between 30 000° K and 7500° K, depending on whether the molecular excitation and reaction rates are infinitely slow or infinitely fast respectively. Figure 1 shows how the concentration of the most important species in the gas at the stagnation point varies along a typical entry trajectory, assuming infinitely

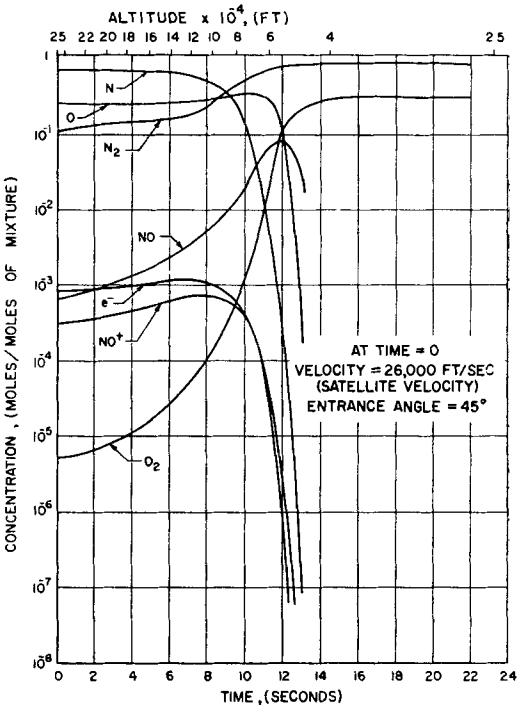

Figure 1. Concentration of the most important chemical species in equilibrium air at the stagnation point for a typical entry trajectory.

fast reaction rates (i.e. equilibrium composition; Gilmore 1955). When we consider the cooling of the gas from the stagnation region as it expands around the body, the question of the rate with which atoms recombine in the inviscid flow and in the boundary layer becomes important. If electromagnetic waves are to be used to send or receive information from a flight object, it is necessary to have an accurate knowledge of the electron

concentration in the inviscid flow. This requires an accurate knowledge of the temperature. A knowledge of the recombination rate is essential if the theory of the inviscid gas flow around the body is to be complete. An important problem, then, is to determine the *dissociation and recombination rates in air.*

The chemical reactions that go on in high temperature air are so complicated that the only reasonable method of approach to the problem, at the present time, is to carry out experiments that simulate the flow situations of interest.

Before discussing the experiments, some of the terminology used in chemical kinetics will be introduced. The recombination of two atoms A, which collide with a third body B to form a molecule A_2, is represented by the relation

$$A + A + B \underset{k_r}{\rightarrow} A_2 + B, \tag{1}$$

where B in the right-hand side is an excited particle which carries away the energy of recombination and k_r is the so-called recombination rate coefficient defined by the differential equation

$$\{d[A]/dt\}_r = -2k_r[A]^2[B], \tag{2}$$

where the square brackets denote concentrations in gm-moles/cm^3, the units of k_r are cm^6 moles^{-2} sec^{-1}, t denotes time, and the subscript r means recombination. Equation (2) says that the time rate of disappearance of atoms is proportional to the concentration of each of the species that take part in three-body collisions. The reaction rate coefficient k_r depends on temperature.

Similarly, the dissociation process is governed by the reverse of (1), and is determined by the dissociation rate constant k_d. (The subscript d will be used again later to denote dissociation.) It should be noted that, in a gas mixture like air, dissociation may occur by other more complicated paths than the one given by the inverse of (2).

In equilibrium chemical thermodynamics (Penner 1955), it is shown that at a given temperature the thermodynamic equilibrium constant K_c is given by

$$k_d/k_r = K_c. \tag{3}$$

(The subscript c denotes that K_c is defined in terms of concentrations.) If one assumes that even in a non-equilibrium state the molecules in their different energy levels have an equilibrium statistical distribution, then (3) still holds.

Knowing the atomic and molecular properties of the species involved in a reaction, K_c can be obtained from statistical mechanical calculations. The values of K_c are well known for the species in air. Therefore, in order to determine the reaction rates, it is necessary to determine experimentally only one of the reaction rates in (3).

2. Chemical kinetic experiments

The shock tube is a useful tool for obtaining air at temperatures and pressures that simulate, in the laboratory, the flight conditions of a body

in hypersonic flight through the atmosphere (Rose & Stark 1957). This air can then be used for the purpose of measuring chemical reaction rates. The basic idea is to cool rapidly, by aerodynamic means, the hot and partially dissociated gas produced in a shock tube. The problem then is to find an observable flow parameter that changes as a function of the chemical reaction rates.

For the purpose of obtaining chemical kinetic data for air, there are two different approaches which can be used. One is to use each of the individual species found in air as a working fluid, in order to investigate the detailed kinetics of each species, and then attempt to reconstruct from that information the more complex behaviour of air. Another approach is to observe the behaviour of the composite gas during rapid changes of state; this last approach is used in the present experiments.

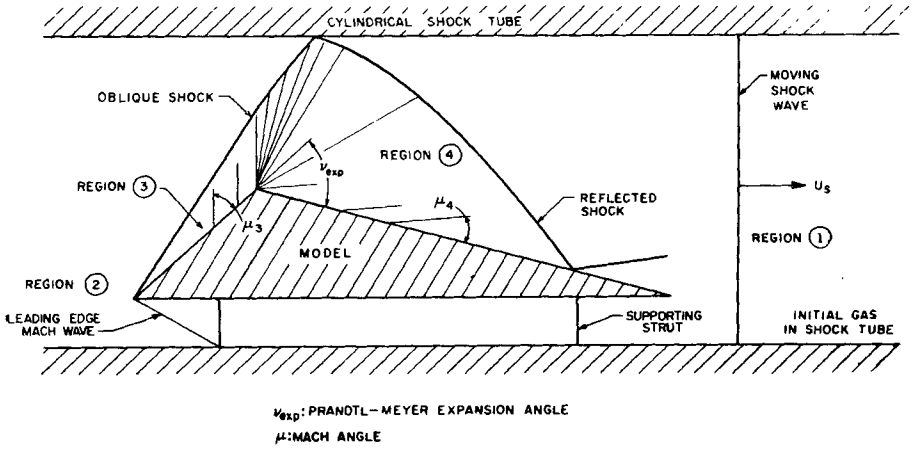

Figure 2. Flow configuration around compression–expansion models.

In one of our experiments, the air behind the moving normal shock is first compressed by means of a wedge (figure 2) spanning the shock tube test section, and is then expanded around a corner (Prandtl–Meyer expansion)*. The two-dimensional model is scribed transversely on the forward and rear surface so that the flow Mach number along the model wall can be determined by taking schlieren photographs of the small disturbances caused by the scratches†. The suddenly cooled gas is then observed as it relaxes towards equilibrium. If the relaxation times are of the appropriate order of magnitude, it would be possible to observe changes of Mach angle with distance along the wall, downstream of the expansion.

* Dr Harry E. Petschek, of the AVCO Research Laboratory, originally suggested the possibility of investigating recombination rates by studying the Prandtl–Meyer expansion of a dissociated gas flowing around a flat plate placed in the shock tube at angle of attack.

† Mach angle measurements have been used in experimental aerodynamics by Hertzberg & Kantrowitz (1950) and by Hertzberg (1956).

This rate of change of Mach angle with distance could be used to calculate the reaction rates. The possible observable difference in Mach angles in region 4 (see figure 2) is largest when the flow upstream of the expansion (region 3) is sonic. The oblique shock compression, then, has the purpose of lowering the Mach number of the initial flow behind the incident shock wave (region 2).

In order to analyse the Prandtl–Meyer expansion in a reacting gas and obtain some understanding of the experimental evidence, it is necessary to know the state of the gas upstream of the expansion. It is therefore important to investigate, first, the flow of air through moving normal shocks in the shock tube, and second, the flow of this shocked air through a standing oblique shock.

3. Experimental determination of the state of the gas behind the incident shock. Flat plate shock tube experiments

The experimental arrangement consists of a flat plate with a sharp leading edge which spans the width of a round shock tube at the point where glass windows have been inserted tangentially to the tube (figure 3).

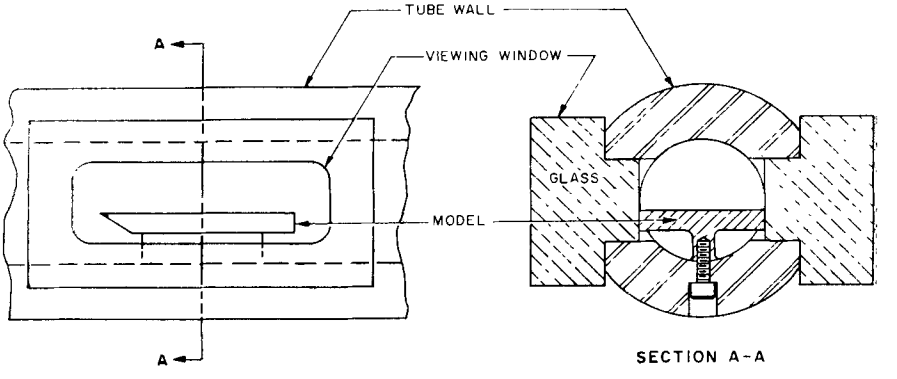

Figure 3. Experimental arrangement of model in schlieren test section in chemical kinetic experiments with the shock tube.

The model is supported by a diamond-shaped strut bolted to the bottom of the test section. Lines perpendicular to the flow are scribed on the model. These lines cause Mach waves in the flow downstream of the incident shock (i.e. in the gas usually used for test purposes; region 1 denotes the undisturbed gas in the shock tube before rupture of the diaphragm). A schlieren photograph of the Mach line pattern of the flow using a model with a highly polished surface and finely scribed lines is shown in figure 4 (*a*) (plate 1). Note the narrow Mach lines coming off the centre portion of the plate. Subsequently, heavier lines were scribed on the same model in addition to the fine lines already there. The result of this change is shown in figure 4 (*b*) (plate 1). Here the heavier lines are seen to fan out. A comparison of the fine and broad waves indicates that the trailing edge

of the strong waves proceeds with the same angle as the weak waves. The result of this comparison becomes useful when interpreting schlieren photographs where only broad waves appear. In figure 4(*c*) (plate 1) a plate scribed so that all lines are identical to each other demonstrates that there is *no measurable Mach number gradient in the flow direction.* The dark lines were drawn at the measured Mach angle to help the visualization of departures from parallelism.

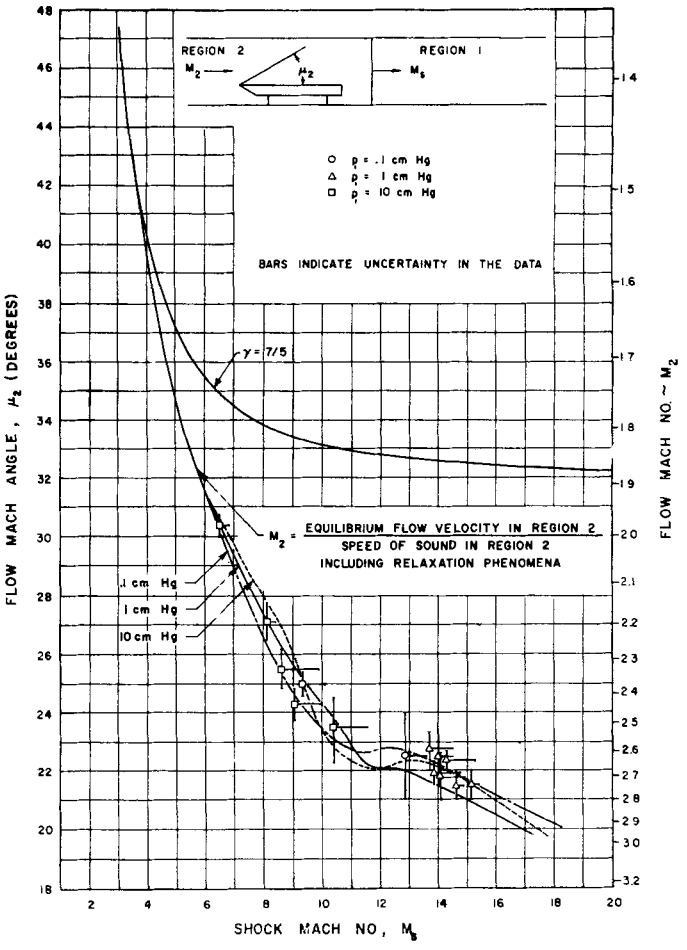

Figure 5. Estimate of flow Mach number downstream of moving shock. (Relaxation phenomena are included when computing sound velocities.) A comparison between frozen flow ($\gamma = 7/5$) and the flat plate Mach line experiments.

It should be remarked that the thickness of the Mach waves can be justified by the finite size of the disturbances and the finite breadth of the test section, and are definitely in no way associated with any relaxation phenomena. Additional experimental confirmation of this fact is given by schlieren photographs of the small disturbances taken in argon in a Mach number range for which no relaxation phenomena occur; the waves appear to have the same thickness as in air.

Since the dissociation rates are not known, the experimental Mach angle μ_2 of the flow downstream of the incident shock is compared (figure 5) with two different theoretical values obtained by making the following two extreme alternative assumptions about the relaxation times and the speeds of sound*:

(*a*) the gas is chemically frozen at room temperature composition, i.e. $\gamma = 7/5$, γ denoting the ratio of specific heats (vibration of the molecules remains unexcited);

(*b*) the flow velocity downstream of the shock is determined by assuming thermodynamic equilibrium across the shock wave, and the choice of the proper speed of sound is determined by the ratio of the vibrational (Blackman 1956) and chemical relaxation times (based on the lower limit of the recombination rates determined in § 6) to the flow times across the Mach waves (cf. Appendix).

The uncertainty in the data shown in figure 5 is due to the spread of the Mach waves, of the order of 1°, and to attenuation of the incident normal shock wave. Figure 5 shows definitely that the dissociation rate is so fast that *the flow in the slug of gas used in our shock tube tests is in thermodynamic equilibrium.* Since the photographs are taken after the incident shock is well out of the field of view, no information was obtained as to the length of the relaxation region in the neighbourhood of the incident shock.

4. Shock tube experiments with wedges

The next question that has to be answered is whether the gas that passed through the incident shock, and which is in thermodynamic equilibrium, will again be in equilibrium when it goes through an oblique shock attached to a wedge located in the shock tube.

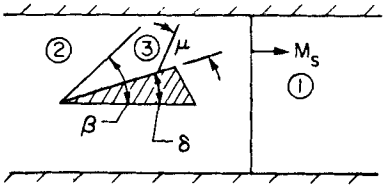

Figure 6. Notation for experiments with wedges.

Experiments have been carried out with wedges, in which the shock angle β was measured as a function of the deflection angle δ (see figure 6). The flow Mach angle μ_3 downstream of the oblique shock (denoted as region 3 in figure 2) was also determined with the scribing technique already mentioned.

A comparison can be made here of the experimental value (β_{exp}) with two different theoretical values of β, obtained by making the following two assumptions:

(*a*) the gas is in chemical equilibrium across the incident shock, and chemically frozen across the oblique shock, but vibration is fully excited (β_{ef});

(*b*) the gas is in equilibrium through both shocks (β_{ee}).

* A discussion of frozen and equilibrium flow, as well as some limiting cases of the speeds of sound in a reacting gas, is given in the Appendix.

The results are given in table 1, where the angles in the columns labelled β_{exp}, β_{ee} and β_{ef} should be compared. There is excellent agreement between the results of the experiments and the calculations assuming full equilibrium.

Run no.	p_1	M_s	δ	β_{exp}	β_{ee}	β_{ef}	μ_{3exp}	$\mu_{3fwr}-\mu_{3exp}$	$\mu_{3fcr}-\mu_{3exp}$	$\mu_{3e}-\mu_{3exp}$
F-145	0·1	15·60	26·0	39·5	39·5	48·1	—	—	—	—
F-146	0·1	16·00	26·0	39·0	39·2	47·9	—	—	—	—
F-70	0·1	14·75	27·0	41·0	41·0	50·2	—	—	—	—
F-141	0·1	14·15	33·0	49·0	49·6	*D*	—	—	—	—
F-74	0·1	12·57	41·0	63·0	63·0	*D*	61·1	3·7	−0·1	−12·3
F-50	0·1	14·15	43·0	63·7	64·3	*D*	69·1	5·0	0·0	−12·0
F-140	0·1	16·90	43·0	59·6	59·4	*D*	—	—	—	—
F-232	1	13·15	20·0	37·5	37·5	40·1	—	—	—	—
F-142	1	13·35	25·0	41·5	41·9	46·6	33·0	2·2	1·0	−2·2
F-143	1	14·60	25·0	40·7	40·7	45·8	33·0	0·4	−0·7	−3·8
F-47	1	13·85	25·7	41·8	42·1	47·3	—	—	—	—
F-129	1	13·65	26·0	43·0	42·4	47·8	—	—	—	—
F-130	1	14·40	26·0	41·5	41·9	47·4	—	—	—	—
F-131	1	14·65	26·0	42·0	41·7	47·2	—	—	—	—
F-133	1	15·15	26·0	40·7	41·2	47·0	—	—	—	—
F-76	1	13·65	26·7	43·3	43·2	48·9	—	—	—	—
F-8	1	14·10	28·8	45·6	45·0	52·1	36·3	1·3	0·0	−3·6
F-53	1	14·85	33·0	50·8	49·4	63·7	—	—	—	—
F-56	1	15·25	36·3	54·0	53·5	*D*	—	—	—	—
F-20	1	14·40	37·0	55·3	55·7	*D*	—	—	—	—
F-19	1	15·30	37·0	54·8	54·5	*D*	44·9	8·1	5·9	−0·2
F-25	1	14·91	38·0	57·0	56·7	*D*	50·7	2·3	0·1	−6·0
F-27	1	14·72	41·0	63·7	63·2	*D*	56·4	3·1	0·0	−7·2
F-54	1	15·65	43·0	67·0	67·1	*D*	—	—	—	—
F-147	10	9·80	20·8	40·0	40·0	41·7	—	—	—	—
F-138	10	8·10	26·0	49·8	50·2	58·2	—	—	—	—
F-144	10	8·10	30·0	56·0	56·3	*D*	—	—	—	—
F-139	10	8·40	30·0	54·9	55·4	*D*	—	—	—	—
F-137	10	8·80	30·0	53·8	53·8	*D*	—	—	—	—
F-136	10	9·80	30·0	52·7	52·3	*D*	—	—	—	—

Table 1. Resumé of oblique shock experiments. p_1 is given in cm Hg, and the angles in degrees. *D* denotes shock detachment.

The last four columns of table 1 give a comparison of the Mach angles μ_{3exp} of the gas flowing over the forward part of the wedge with the theoretical values obtained by using three different speeds of sound. The indication is that of these three speeds of sound, the one that gives best

agreement with experiments is the speed of sound a_{fcv} calculated by freezing the chemical composition at the equilibrium value behind the oblique shock and by letting the vibration participate in the changes across a sound wave. The reason why the Mach angle μ_3 is so sensitive to the different speeds of sound (see the last four columns of table 1) is that the flow over the wedges is only slightly supersonic. On the other hand, this transonic flow is also sensitive to boundary layer constrictions in the shock tube; these may cause the flow not to be truly steady and two-dimensional, and consequently, introduce the longitudinal gradients that were observed in some cases. Also, it should be pointed out that a 1% uncertainty in the shock Mach number M_s produces a 2% error in the Mach number M_3 of the flow over the wedge. Since the experiments are performed in a heated gas produced by an attenuating shock, the conclusions drawn from the Mach number measurements in region 3 may still be opened to question. The effect that these gradients have on the flow after the Prandtl–Meyer expansion (region 4 in figure 2) can be shown to be negligible.

Evidence of the steadiness of the flow around the models in the shock tube has been obtained by taking drum camera photographs of the self-luminosity of the flowing gas. On the outside surface of the window (figure 3) a slit is positioned with respect to the compression–expansion model, as indicated on the lower portion of figure 7 (plate 2). Note in the upper portion of the figure (which is the drum camera photograph) that after the first 10 μsec the oblique shock remains in a steady position for approximately 20 μsec; a sufficient time to gather experimental data. This time, called the testing time, is a function of p_1, M_s and shock tube length.

From the evidence given in the last two sections, it may be concluded that *the gas upstream of the Prandtl–Meyer expansions is in thermodynamic equilibrium.* This is the information needed as a starting point for the interpretation of the recombination experiments.

5. Prandtl–Meyer expansion experiments

A typical schlieren photograph of the air flow about the compression–expansion models is given in figure 8 (plate 3). The calculated shock angle can be seen to agree with the experimental one*. The oblique shock

* The shock curvature upstream of the start of the Prandtl–Meyer expansion is due to an expansion wave which comes from the upper-left corner of the flow field, where the viewing window joins the shock tube (cf. figures 3 & 4 (*a*) (plate 1)). The experiments reported here have been repeated in a square cross-sectional test-section, the windows and walls being on the same plane, and no premature curvature of the oblique shock was detected.

The flow along the model wall, downstream of the expansion, is not affected by the tube-window-joint expansion. The reason for not publishing the schlieren photographs taken in the square section is that the lines downstream of the Prandtl–Meyer expansion were not defined well enough to be reproduced clearly by the photo-offset method.

appears to have a large thickness because the boundary layer on the windows thickens along the intersection with the shock plane. The oblique shock is reflected by the cylindrical wall of the tube. The Mach lines, produced by scribing the model, are clearly seen on the back surface and faintly on the front wedge.

In all the experiments that have been carried out, no measurable variation has been found in the Mach angle of the flow downstream of the Prandtl–Meyer expansion. This means that we are dealing with either the extreme cases in which the gas is chemically frozen across the expansion, or that in which all the recombination has taken place by the time the gas emerges from the last wave of the expansion fan. It will now be necessary to calculate the Prandtl–Meyer expansion for the extreme cases of either frozen flow or equilibrium flow.

For *chemically frozen flow*, the two values of γ from (A.5) and (A.7) of the Appendix can be used first to determine the speed of sound behind the oblique shock, and then to calculate the Mach number M_3 in this region. (Although the differences between the two Mach numbers and the experimental value are small, one value consistently agrees better with experiment than the other.) Starting with the Mach numbers just determined (γ and the expansion angle ν are known) it is possible to calculate, using the usual Prandtl–Meyer formulae, two possible Mach numbers for the chemically frozen flow after the expansion, M_{4fnv} (frozen, no vibration) and M_{4fcv} (frozen, classical vibration). A typical result for frozen flow, classical vibration, is shown in figure 8 (plate 3) where it can be seen that the calculated Mach angle (black lines) is very different from the experimental one (white waves). If the vibration were also assumed to be frozen, the lack of agreement would be greater.

The alternative extreme case is obtained if we assume that the recombination rate is infinitely fast, and that *the flow is in equilibrium* beyond the expansion. It can be shown, by writing the usual relation

$$d\nu = \sqrt{(M^2-1)}\, du/u$$

in terms of enthalpy, that the condition after an expansion of ν radians is given by the integral equation

$$\nu = \frac{1}{2}\int_{H_3}^{H_4}\left[\left(\frac{u}{a}\right)^2 - 1\right]^{1/2}\frac{dH}{H} = \frac{1}{2}\int_{H_3}^{H_4}\left(\frac{2H}{a^2} - 1\right)^{1/2}\frac{dH}{H}, \tag{4}$$

evaluated along an isentrope, where $H = h_t - h = \frac{1}{2}u^2$, h_t, h and u denote, respectively, total enthalpy of the flow, local enthalpy, and velocity in the expansion, a is the local speed of sound, and subscripts 3 and 4 denote conditions before and after the expansion respectively. For the purpose of integrating (4), it is convenient to have a Mollier chart that has lines of constant equilibrium speed of sound a_e, as given by (A.9). When the integral is evaluated (numerically or graphically) it is possible to plot the expansion angle ν *vs* the full equilibrium Mach number M_{4ee}, where

$$M_{4ee} = \sqrt{(2H)}/a_e. \tag{5}$$

Entering this plot with the experimental expansion angle ν_{exp}, the value of M_{4ee} for the particular experiment can be determined.

If one assumes that the characteristics in a supersonic stream of reacting gas propagate with the equilibrium speed of sound, but that a finite disturbance could travel with the 'locally' frozen speed of sound, it is possible to obtain two other Mach numbers for the expanded flow. The value of ν obtained from (4) by using a_e may be plotted alternatively *vs* $\sqrt{(2H)}/a_{fnv}$ and *vs* $\sqrt{(2H)}/a_{fcv}$*; this leads to M_{4efnv} and M_{4efcv}. There are, therefore, depending on the relaxation times that are unknown, five possible ways of computing the flow Mach number. They give M_{4fnv}, M_{4fcv}, M_{4efnv}, M_{4efcv}, M_{4ee}. These are then compared with the experimental value M_{4exp}. In figure 9 (plate 3), the calculated Mach lines that agree best with the experimental values (they correspond to M_{4efcv}) have been superposed on the photograph; the agreement is very good.

It should be emphasized that in all the Mach numbers that contain an *e* in their subscripts, the relation between ν and μ is obtained assuming thermodynamic equilibrium. The three different Mach numbers M_{4efnv}, M_{4efcv} and M_{4ee} differ only in the manner in which the corresponding speed of sound is defined.

Run no.	p_1	Ms	δ	β_{exp}	β_{th}	ν	μ_{4exp}	$\mu_{4fnv}-\mu_{4exp}$	$\mu_{4fcv}-\mu_{4exp}$	$\mu_{4ee}-\mu_{4exp}$	$\mu_{4efnv}-\mu_{4exp}$	$\mu_{4efcv}-\mu_{4exp}$
F-135	0·1	15·25	40·0	55·0	56·0	50·0	25·7	−11·0	−9·7	−5·0	−1·8	−2·7
F-74	0·1	12·57	41·0	63·0	63·0	56·2	20·1	−5·2	−3·5	0·8	1·6	2·7
F-50	0·1	14·15	43·0	63·7	64·3	58·0	23·8	−9·8	−8·0	−3·0	0·0	−0·9
F-142	1	13·35	25·0	41·5	41·9	58·0	16·8	−7·8	−5·2	−1·7	−0·3	−1·0
F-143	1	14·60	25·0	40·7	40·7	58·0	16·5	−1·9	0·3	−1·7	−0·1	−0·7
F-8	1	14·10	28·8	45·9	45·0	43·4	19·0	−4·3	−3·0	−0·3	2·1	2·3
F-25	1	14·91	38·0	57·0	56·7	50·0	21·9	−6·5	−5·1	−1·1	2·2	1·0
F-122	1	15·00	40·1	59·9	60·1	50·0	24·3	−7·6	−6·0	−1·7	1·5	0·5
F-27	1	14·72	41·0	63·7	63·2	53·0	23·6	−8·5	−7·0	−2·7	0·3	−0·6

Table 2. Mach angles after Prandtl–Meyer expansion. A comparison between experiments and theory. The notation is given in figure 2.

The region in a Mollier diagram covered by the compression–expansion experiments is shown in figure 10, where the stagnation conditions have been plotted for the trajectories of several bodies of possible interest.

The significant data in these experiments, and the results of calculations for the flow Mach angle after the Prandtl–Meyer expansion, are presented in table 2. A comparison of the last five columns shows that, except for small wedge angles where the experiment is insensitive, *the flow Mach angle μ_4 is significantly closer to the calculated equilibrium values.* The speed of sound in the reacting gas used in the equilibrium calculations which agree best with the experimental results seems to be

$$a_{fnv} = \gamma_{nv} ZRT, \quad \text{where } \gamma_{nv} = \frac{4+3Z}{4+Z}.$$

* The notation used for the speeds of sound is given in the Appendix.

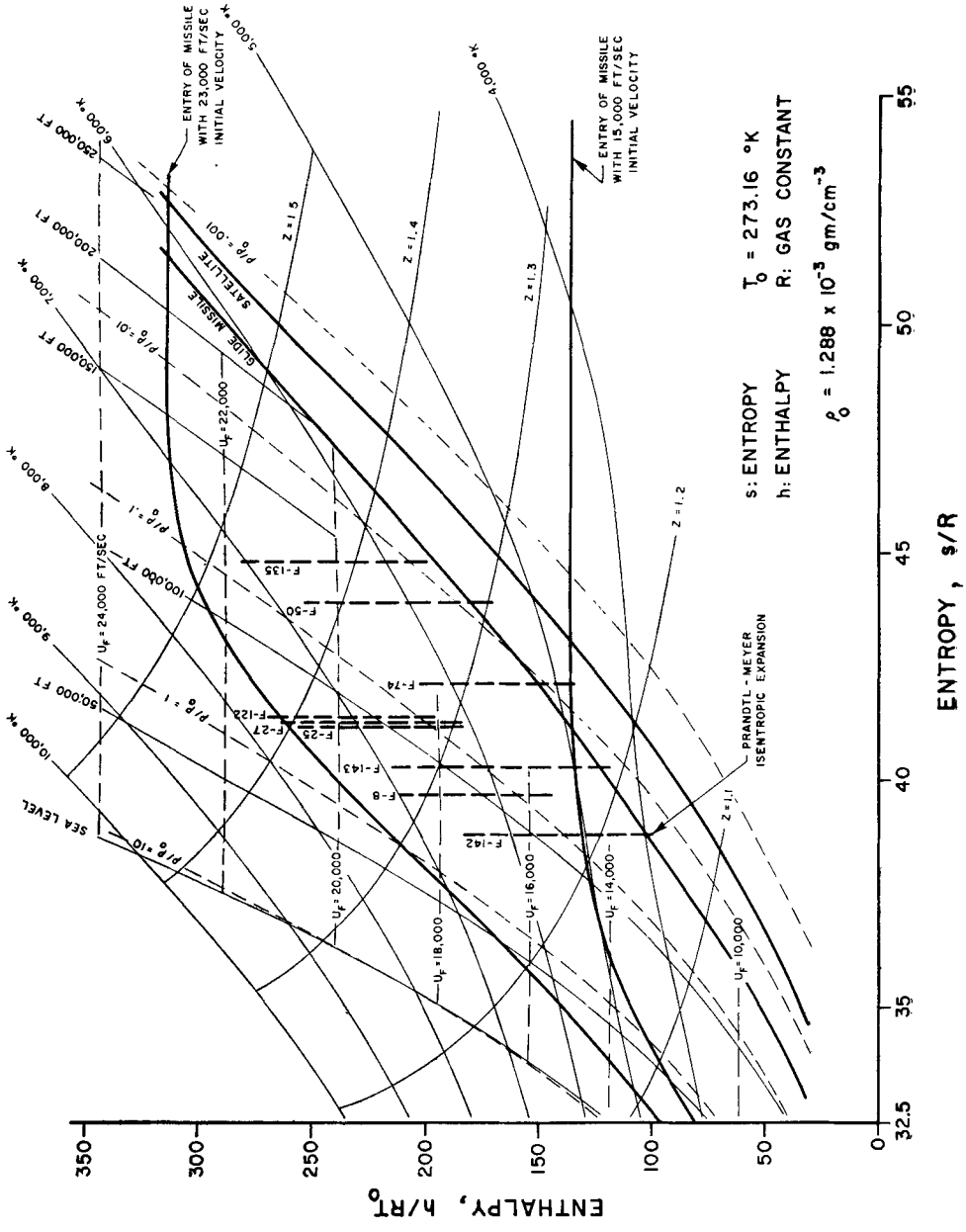

Figure 10. Comparison between the state of gas at the stagnation point of several bodies, and the Prandtl–Meyer expansion in the chemical kinetic experiments with air.

The fact that the experiments agree better with the speed of sound without excitation of the vibration of the molecules is in agreement with Blackman's vibrational relaxation times (although in the present case we also have the possibility of chemical reaction). These times, when compared with the times for a gas particle to traverse the thickness of one of the disturbances used to determine the flow Mach number in region 4 of figure 2, show that the vibration should be frozen in the present measurements.

On the other hand, if the flow around the expansion, as close to the corner as can be measured, is in chemical equilibrium, it does not seem plausible that the flow across a sound wave should be chemically frozen. Since the experimental angles that appear in the schlieren photographs are not sufficiently sharp, the use of the speed of sound defined by the last equation cannot be defended too strongly.

The question concerning the proper speed of sound to use in the equilibrium calculations is a difficult one to answer with the present evidence. Regardless of the outcome, *the data indicate that the flow is definitely not frozen but maintains a state very close to equilibrium.*

6. Estimate of a lower limit for the recombination rate

From the Prandtl–Meyer expansion experiments, it is possible to estimate a lower limit for the recombination rate. An analytic expression which will permit us to do this calculation will now be derived.

The rate equation (2) will be rewritten in terms of weight fractions defined by

$$y_i = \frac{\text{gm of species } i \text{ per unit volume}}{\text{gm of mixture per unit volume}}.$$

Subscripts a and m will denote atoms and molecules respectively. Since $y_a + y_m = 1$, we have

$$[A] = \rho y_a / W_a, \quad [A_2] = \rho y_m / W_m, \quad [B] = [A] + [A_2] = \rho(1+y_a)/W_m, \tag{6}$$

where ρ is the gas density and W_m the molecular weight of undissociated gas. The insertion of (6) into (2) yields

$$\{dy_a/dt\}_r = -(2\rho/W_m)^2 k_r y_a^2 (1+y_a). \tag{7}$$

If account is also taken of the dissociation reaction

$$A_2 + B \underset{k_d}{\rightarrow} A + A + B,$$

the net rate can be expressed as

$$dy_a/dt = \{dy_a/dt\}_d + \{dy_a/dt\}_r. \tag{8}$$

The reaction rate for dissociation can be expressed as

$$\{d[A]/dt\}_d = 2k_d[A_2][B] = 2k_d(\rho/W_m)^2(1-y_a^2), \tag{9}$$

which together with (7) can be inserted in (8) to yield

$$dy_a/dt = (\rho/W_m)^2(1+y_a)[2k_d(1-y_a) - 4k_r y_a^2]. \tag{10}$$

At equilibrium $dy_a/dt = 0$, and the above expression gives

$$k_d = 2k_r y_{ae}^2/(1-y_{ae}) \tag{11}$$

which, together with (10), gives for the recombination rate k_r

$$k_r = \left(\frac{W_m/2\rho_0}{\rho/\rho_0}\right)^2 \frac{u\, dy_a/dx}{(1+y_a)[y_{ae}^2(1-y_a)/(1-y_{ae})-y_a^2]}, \tag{12}$$

where x denotes length measured along a streamline and u is the flow velocity.

Since the atomic weight fraction y_a is given in terms of the compressibility Z by

$$y_a = Z-1,$$

equation (12) may be written as

$$k_r = \left(\frac{W_m/2\rho_0}{\rho/\rho_0}\right)^2 \frac{u(dZ/dv)(dv/dx)}{Z[(Z_e-1)^2(2-Z)/(2-Z_e)-(Z-1)^2]}, \tag{13}$$

where v is the Prandtl–Meyer expansion angle.

Equation (13) can be used for an order of magnitude calculation in the following way. We will choose a streamline 1 mm away from the forward wedge wall (this being the closest to the wall of those streamlines that

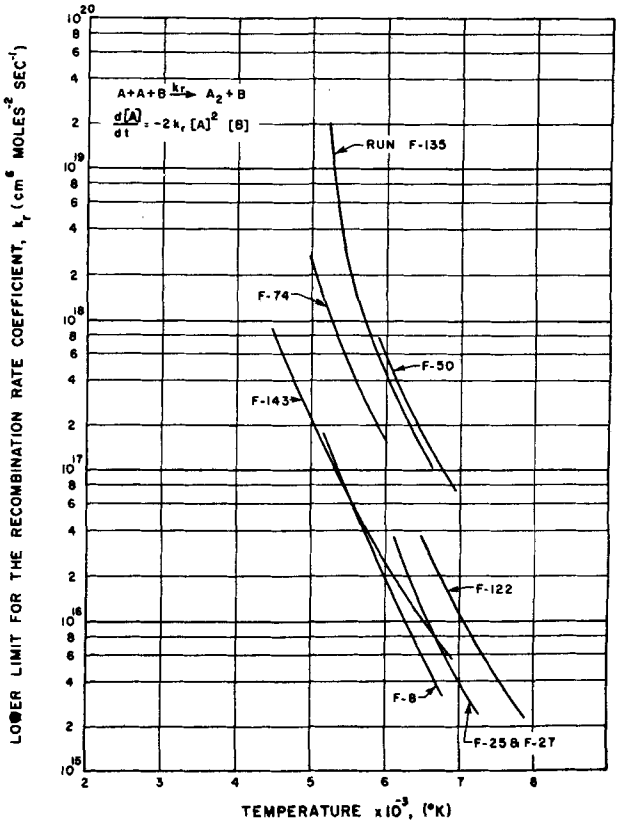

Figure 11. Lower limit for the recombination rate coefficient obtained from the Prandtl–Meyer expansion experiments.

can be seen flowing around the corner in the schlieren photographs), and follow it around the Prandtl–Meyer expansion. Consider the flow through a small expansion angle $\Delta\nu$. The problem is to decide what to use for Z and Z_e in (13). Since the experimental evidence is that after any expansion we get equilibrium, the value of Z_e to be used in (13) should be the equilibrium value *after* the expansion. On the other hand, since there is no experimental evidence for the value of Z *within* the expansion, we could assume, as an extreme condition, that Z stays at the equilibrium value at the *beginning* of the expansion. Any other choice of Z would give a larger value of k_r. Thus, the values of k_r calculated by using the local properties of the gas through the expansion are a *lower limit for the recombination rates.* The results are given in figure 11 as a function of temperature. These experiments have covered roughly a density range of standard to 1/200 of standard density.

The chemical kinetic theory that interprets the experimental results still remains to be developed.

7. Conditions for thermodynamic equilibrium in flight

Let the criterion for equilibrium flow require that the time for a gas particle to traverse the body length is ten times the chemical relaxation time. Making use of the relation

$$k_r \geqslant 10^{18} \text{ cm}^6 \text{ mole}^{-2} \text{ sec}^{-1}, \tag{14}$$

it is possible, when adopting the equality sign in the recombination rate of (14), to find an altitude (for a given body) below which the flow will stay in thermodynamic equilibrium as it flows around the body, provided the gas behind the detached shock is in equilibrium. (The effect of other limiting values of k_r will be discussed later.) This has been done for blunt bodies of 1 and 10 ft. surface length (figure 12). If the stagnation point gas is in thermodynamic equilibrium, the shaded area covers the region where the flow around a 1 ft. body may be expected to be in equilibrium. The corresponding result for a 10 ft. body is also given in figure 12. The shape and location of the two curves are insensitive to body shape, provided the body is blunt and smooth. The curves of $y_{ae} = \text{const.}$ indicate the flight conditions at which the air at the stagnation point of a blunt body has a noticeable degree of dissociation. If a recombination rate k_r larger by a factor of 10 be adopted, the effect on the curve for the 1 ft. body is to displace it to where the 10 ft. curve is now. On the other hand, if the criterion for equilibrium flow requires the flow transit time to be 100 times the relaxation time (instead of 10), the 1 ft. curve is displaced downward in figure 12 by approximately 40 000 ft. Several typical trajectories (Masson & Gazley 1956) have also been included in figure 12. It can be seen that the flow around a satellite entering the atmosphere may not be in thermodynamic equilibrium. This points towards the importance of designing chemical kinetic experiments on a faster time scale than for those described here.

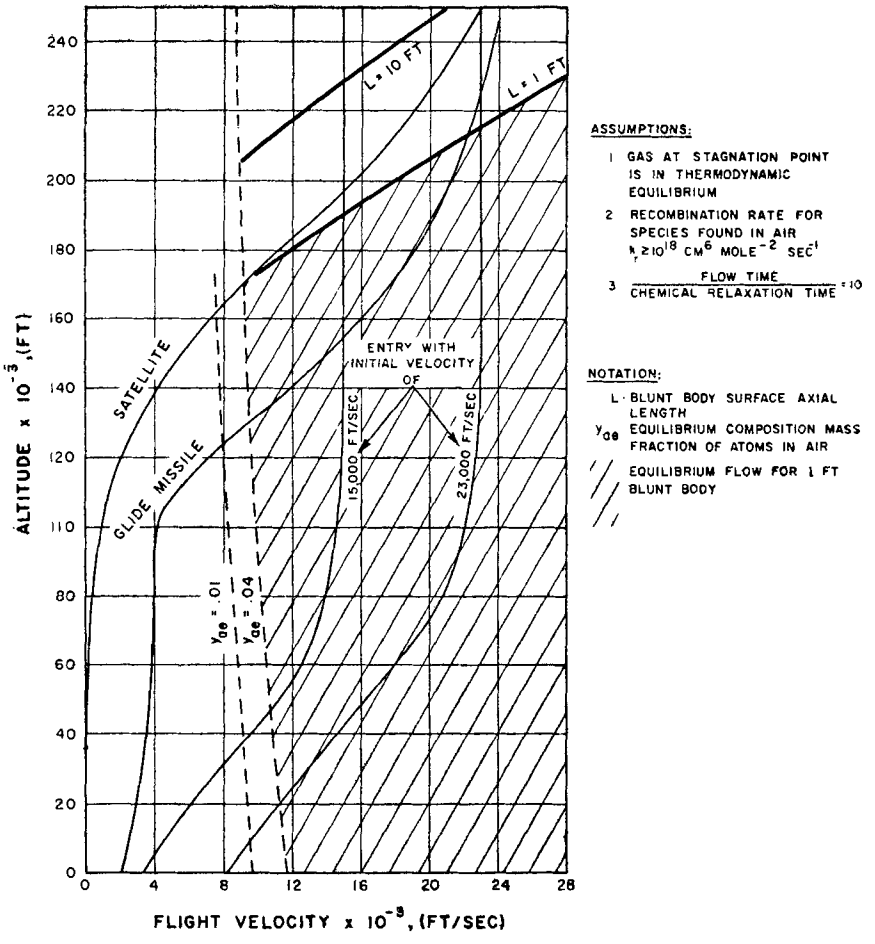

Figure 12. Flight conditions for which equilibrium flow may be expected around a blunt body. Some typical trajectories for bodies entering the atmosphere are also shown.

This work has been sponsored by the Ballistic Missile Division, Air Research and Development Command, U.S. Air Force, under contract AF04(645)–18. The author wishes to express his appreciation to the staff members of the AVCO Research Laboratory who contributed to this work, especially to Dr Arthur Kantrowitz, director of the laboratory, and to Professor James A. Fay, of the Massachusetts Institute of Technology and consultant to AVCO, for helpful discussions during the course of this work. Thanks are due to Mr James E. Trider for having carried out the shock tube experiments, and without whose cooperation and enthusiasm the experimental work would have not progressed to the stage reported here.

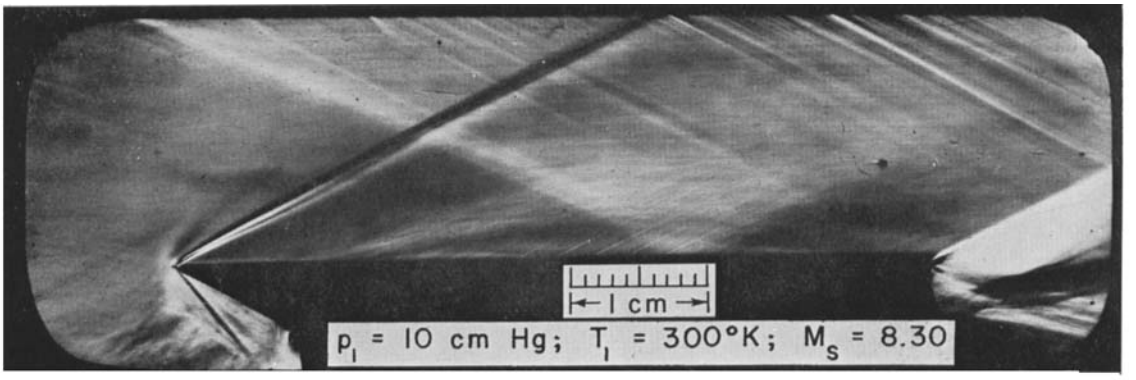

(*a*) Model scribed with very fine lines.

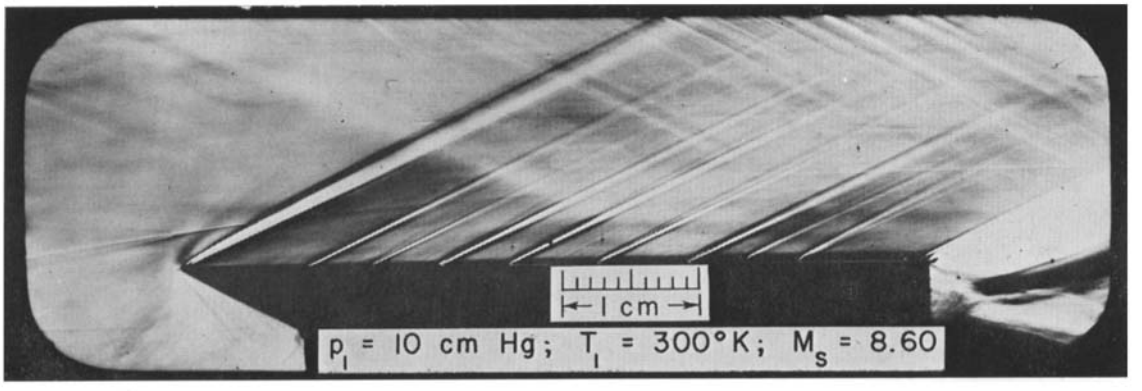

(*b*) Heavy lines scribed in addition to fine lines of figure 4 (*a*).

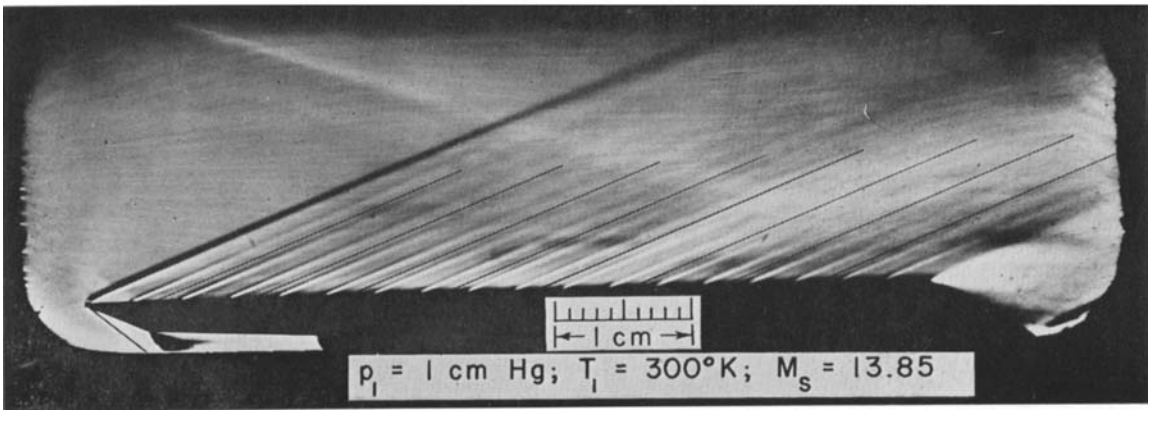

(*c*) Model scribed with heavy lines identical with each other.

Figure 4. Flow over flat plates in the shock tube. Subscript 1 refers to region 1 in figure 2. M_s is the ratio of the shock velocity to the speed of sound in region 1.

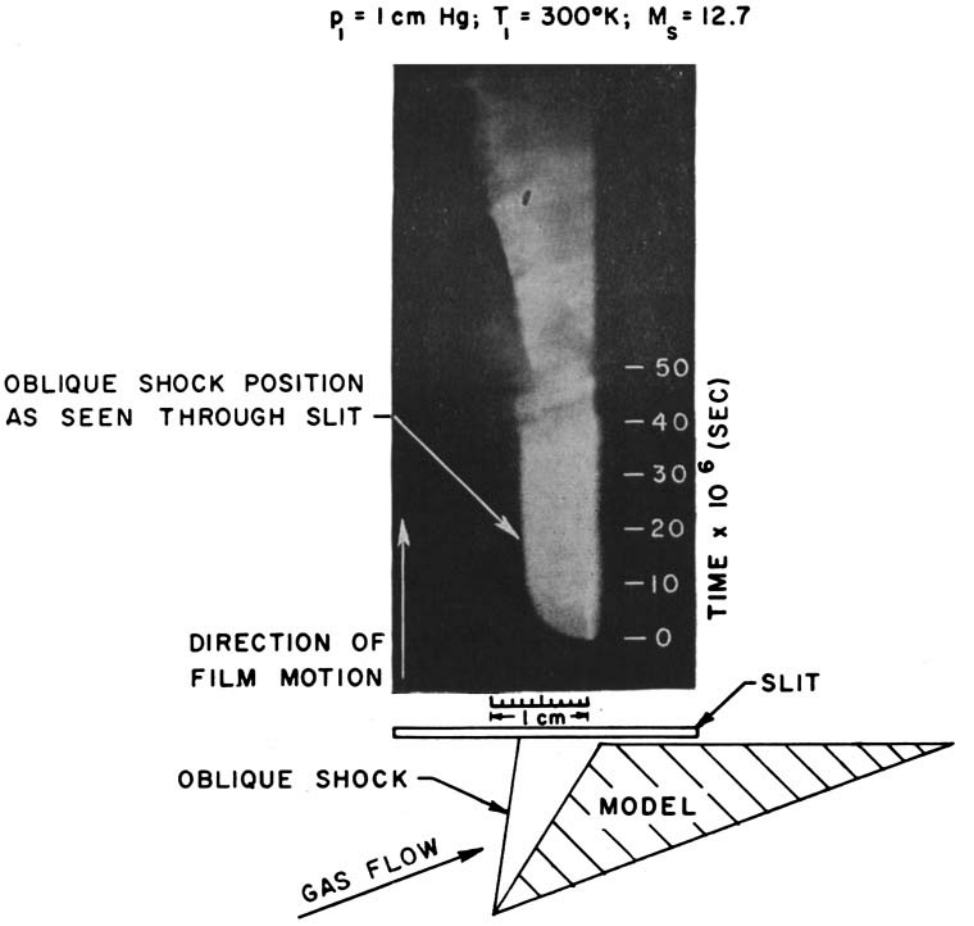

Figure 7. Drum camera photograph of flow around wedge.

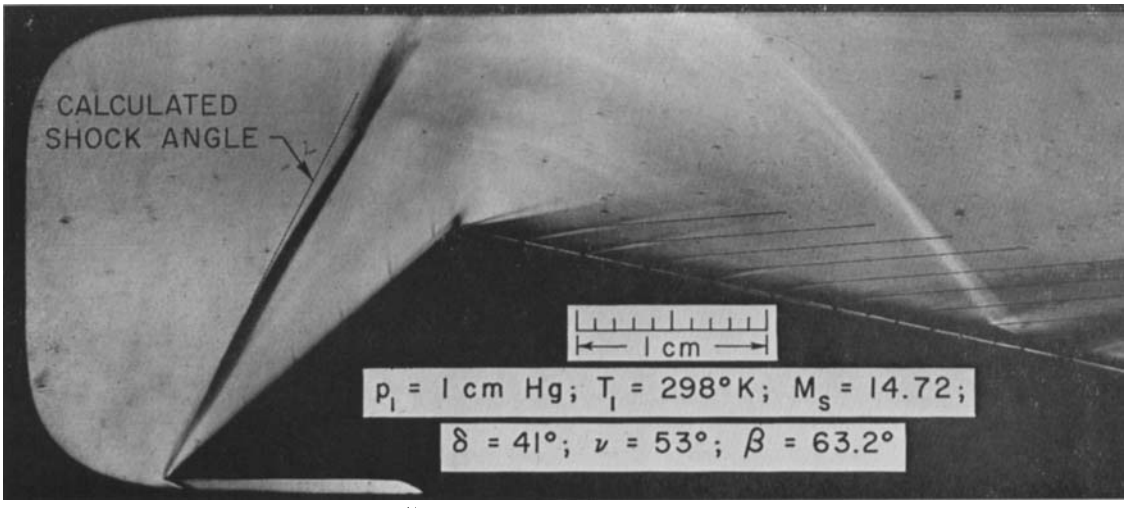

Figure 8. Comparison with experiment of Mach lines for frozen flow, classical vibration. ($\gamma = 1{\cdot}375$, $M_{4fnv} = 3{\cdot}50$, $\mu_{4fnv} = 16{\cdot}6°$.)

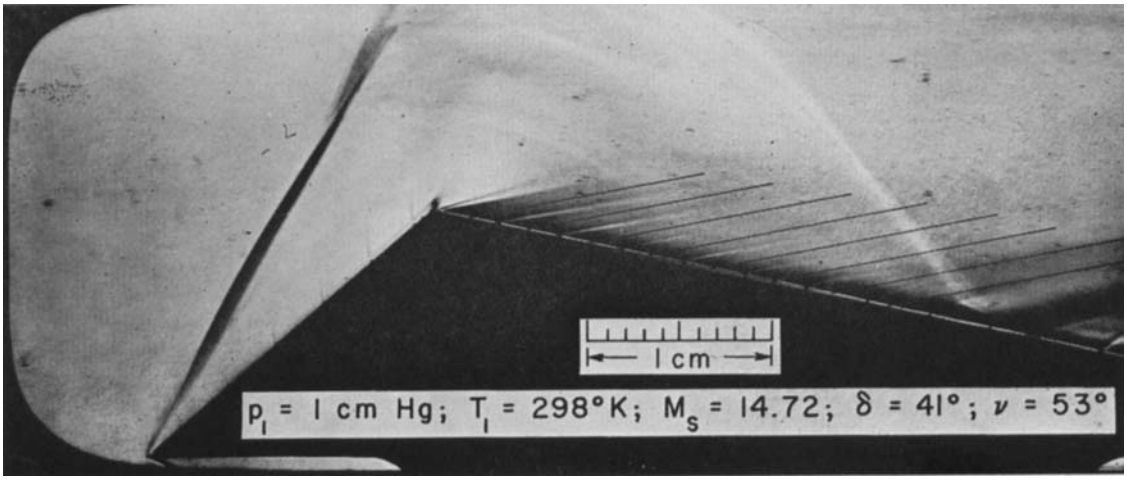

Figure 9. Comparison with experiment of Mach lines for equilibrium velocity and frozen speed of sound, classical vibration. ($M_{4efcv} = 2{\cdot}56$, $\mu_{4efcv} = 23{\cdot}0°$.)

Appendix. Frozen and equilibrium flow. Some limiting cases of the speed of sound in a reacting gas

The speed with which a small disturbance, called a sound wave, propagates in a reacting gas is known to depend on the rates at which the atomic and molecular internal degrees of freedom can adjust themselves to small changes in the thermodynamic coordinates. If the gas is chemically reactive, the sound speed depends also on the reaction rates, or the chemical relaxation times. The relaxation time τ for a process is defined by

$$\frac{1}{\tau} = \frac{1}{y-y_e}\frac{d(y-y_e)}{dt}, \tag{A.1}$$

where y may denote instantaneous concentration in the case of chemical reactions, or energy in the case of energy excitation of external or internal degrees of freedom. The subscript e denotes the equilibrium value of y. The value of τ is constant when the process involved is exponential, i.e. near equilibrium.

If the typical time necessary for a particle of gas to flow over a body of interest is denoted by τ_{flow} and if

$$\tau_{\text{flow}}/\tau \ll 1, \tag{A.2}$$

the flow is called *frozen flow*, i.e. no reaction occurs during the time a particle spends flowing over the body. Conversely, *equilibrium flow* is defined by

$$\tau/\tau_{\text{flow}} \ll 1. \tag{A.3}$$

Frozen and equilibrium flow having been defined, the discussion that follows will be concerned with the speeds of sound. It will be implied that the rotational relaxation times, for the diatomic molecules in air, are negligibly small when compared with the vibrational and chemical relaxation times (Hertzfeld 1955). The vibrational relaxation times in pure oxygen and nitrogen and their mixtures have been measured by Blackman (1956). There are four possibilities of interest for the speeds of sound, and two for the ratio of specific heats γ.

(*a*) The chemical reaction rate is very slow, no change in composition occurring across a sound wave, and the rotation of the molecules participates in the change, but the vibration of the molecules does not. The speed of sound so defined will be called *frozen speed of sound, frozen vibration.* Its value can be shown to be

$$a_{fnv}^2 = \gamma_{nv} ZRT, \tag{A.4}$$

where $Z = p(\rho RT)^{-1}$ gives a measure of the degree of dissociation of the gas (Z can be obtained from a Mollier chart for equilibrium air, Feldman 1957), R is the undissociated gas constant, and λ_{nv} the ratio of specific heats* is defined by

$$\gamma_{nv} = \frac{4+3Z}{4+Z}. \tag{A.5}$$

* The specific heat ratio can be obtained by writing the expressions for the enthalpy and internal energy of a mixture of atoms and diatomic molecules, and taking their derivatives with respect to temperature to obtain the specific heats.

(*b*) The same as case (*a*), except that here vibration participates in the changes in a sound wave (i.e. the vibrational relaxation times are very short). This sound speed will be called *frozen speed of sound, equilibrium vibration.* For the purpose of calculation, it will be assumed that the contribution of the vibrational degree of freedom to the heat capacities is the classical value RT, which is nearly true for the conditions of interest. This speed of sound will be called *frozen speed of sound, classical vibration,* and is given by

$$a_{fcv}^2 = \gamma_{cv} ZRT, \tag{A.6}$$

where the ratio of specific heats γ_{cv} is

$$\gamma_{cv} = \frac{8+Z}{8-Z}. \tag{A.7}$$

(*c*) The chemical reaction rates and the excitation of the rotation of the molecules are infinitely fast. Vibration of the molecules does not participate. This sound speed is called *equilibrium speed of sound, frozen vibration,* and is defined by

$$a_{env}^2 = (\partial p/\partial \rho)_{s = \text{const.}}, \tag{A.8}$$

where $\partial p/\partial \rho$ could be evaluated, along an isentrope, on a Mollier chart which includes a fixed value for the vibrational energy of the molecules.

(*d*) The chemical reaction rates, rotation and vibration are fast enough to follow completely the changes in a sound wave. This is the *full equilibrium speed of sound* and is found from the usual expression

$$a_e^2 = (\partial p/\partial \rho)_{s = \text{const.}}. \tag{A.9}$$

The relative magnitudes of these speeds of sound are

$$a_{fnv} < a_{fcv} < a_{env} < a_e, \tag{A.10}$$

the difference between the extreme values being of the order of 10 to 20% in the range of temperatures encountered in hypersonic flight.

References

Blackman, V. 1956 *J. Fluid Mech.* **1**, 61.

Feldman, S. 1957 Hypersonic gas dynamic charts for equilibrium air, *Avco Research Laboratory Handbook.*

Gilmore, F. R. 1955 Equilibrium composition and thermodynamic properties of air to 24,000° K, *Rand Corp., Report* no. RM–1543.

Hertzberg, A. & Kantrowitz, A. R. 1950 *J. Appl. Phys.* **21**, 874.

Hertzberg, A. 1956 *Jet Propulsion* **26**, 549.

Hertzfeld, K. F. 1955 Relaxation phenomena in gases, section H of *Thermodynamics and Physics of Matter.* Princeton University Press.

Masson, D. J. & Gazley, C. 1956 *Aero. Eng. Rev.* **15**, 46.

Penner, S. S. 1955 Introduction to the study of chemical reactions in flow systems, *AGARDograph* no. 7. London : Butterworths Scientific Publications.

Rose, P. H. & Stark, W. I. 1957 *J. Aero. Sci.* (to be published).